British Journal of Pharmacology

DOI:10.1111/j.1476-5381.2011.01274.x
www.brjpharmacol.org

RESEARCH PAPER

The cardioprotective efficacy of TVP1022 in a rat model of ischaemia/reperfusion

Offir Ertracht[1,2]*, Esti Liani[1,2]*, Noa Bachner-Hinenzon[4], Orit Bar-Am[3], Luba Frolov[1,2], Elena Ovcharenko[1,2], Huda Awad[1], Shany Blum[2,5], Yaron Barac[1,2], Tamar Amit[3], Dan Adam[4], Moussa Youdim[3] and Ofer Binah[1,2]

[1]*Department of Physiology,* [2]*Ruth and Bruce Rappaport Family Institute for Research in the Medical Sciences,* [3]*Department of Pharmacology, Ruth and Bruce Rappaport Faculty of Medicine,* [4]*Faculty of Biomedical Engineering,* [5]*Department of Anatomy and Cell Biology, Technion-Israel Institute of Technology, Haifa, Israel*

Correspondence
Ofer Binah, Department of Physiology, Ruth and Bruce Rappaport Faculty of Medicine, Technion – Israel Institute of Technology, PO Box 9649, Haifa 31096, Israel. E-mail: binah@tx.technion.ac.il

*These authors contributed equally to the manuscript.

Keywords
myocardial infarction; ischaemia/reperfusion injury; cardioprotection; TVP1022; cardiomyocytes

Received
7 September 2010
Revised
28 December 2010
Accepted
5 January 2011

BACKGROUND AND PURPOSE

Because myocardial infarction is a major cause of morbidity and mortality worldwide, protecting the heart from the ischaemia and reperfusion (I/R) damage is the focus of intense research. Based on our *in vitro* findings showing that TVP1022 (the S-enantiomer of rasagiline, an anti-Parkinsonian drug) possesses cardioprotective effects, in the present study we investigated the hypothesis that TVP1022 can attenuate myocardial damage in an I/R model in rats.

EXPERIMENTAL APPROACH

The model consisted of 30-min occlusion of the left anterior descending artery followed by 4 or 24 h reperfusion. In addition, we investigated the possible mechanisms of cardioprotection in H9c2 cells and neonatal rat ventricular myocytes (NRVM) exposed to oxidative stress induced by H_2O_2.

KEY RESULTS

TVP1022 (20 and 40 mg·kg^{-1}) administered 5 min before reperfusion followed by an additional dose 4 h after reperfusion reduced the infarct size and attenuated the decline in ventricular function. TVP1022 also attenuated I/R-induced deterioration in cardiac mitochondrial integrity evaluated by mitochondrial swelling capacity. *In vitro*, using H9c2 cells and NRVM, TVP1022 attenuated both serum free- and H_2O_2-induced damage, preserved mitochondrial membrane potential and Bcl-2 levels, inhibited mitochondrial cytochrome *c* release and the increase in cleaved caspase 9 and 3 levels, and enhanced the phosphorylation of protein kinase C and glycogen synthase kinase-3β.

CONCLUSIONS AND IMPLICATIONS

TVP1022 provided cardioprotection in a model of myocardial infarction, and therefore should be considered as a novel adjunctive therapy for attenuating myocardial damage resulting from I/R injuries.

Abbreviations

ΔΨm, mitochondrial membrane potential; DAPI, 4′,6-diamidino-2-phenylindole; EF, ejection fraction; FS, fractional shortening; GSK-3β, glycogen synthase kinase 3β; I/R, ischemia/reperfusion; JC-1, 5,5′,6,6′-tetrachloro-1,1′,3,3′-tetraethyl-benzimidazolylcarbocyanine iodide; LVIDs/d, left ventricle intraventricular diameters of systole and diastole; MPTP, mitochondrial permeability transition pore; MTT, 3-(4.5-dimethylthiazol-2-yl)-2.5-diphenyltetrazolium; NRVM, neonatal rat ventricular myocytes; PI3K, phosphoinositide 3 kinase; PMA, 12-myristate 13-acetate; ROS, reactive oxygen species; STE, speckle tracking echocardiography

Introduction

As myocardial infarction is a major cause of morbidity and mortality worldwide (Tiyyagura and Pinney, 2006; Lloyd-Jones *et al.*, 2009), protecting the heart from ischaemia and reperfusion (I/R) damage is the focus of intense research. However, despite numerous publications and many successful preclinical experiments, thus far, no effective cardioprotective drug has found its way into clinical practice (Black, 2000; Downey and Cohen, 2009). In view of such shortage of effective drugs for attenuating I/R damage, we have been studying the cardioprotective efficacies of TVP1022 [the S-enantiomer of rasagiline (Azilect®), an anti-Parkinsonian drug] in a variety of *in vitro* experimental models. In agreement with its cytoprotective efficacy, TVP1022 protected neonatal rat ventricular myocytes (NRVM) against doxorubicin- and serum starvation-induced apoptosis (Kleiner *et al.*, 2008). TVP1022 also attenuated the functional (e.g. intracellular Ca^{2+} transients, contractions, intercellular coupling) derangements in NRVM exposed to doxorubicin (Berdichevski *et al.*, 2010). Although TVP1022 is 1000-fold less active than rasagiline as a MAO inhibitor (Mandel *et al.*, 2005; Youdim *et al.*, 2005), it exerts a prominent neuroprotective effect in neuronal cell cultures in response to various neurotoxins and also shows neuroprotection in an *in vivo* model of head trauma (Huang *et al.*, 1999; Youdim *et al.*, 2001; 2005). Studies on the structure-activity relationship of TVP1022 revealed that the neuroprotection is associated with its propargyl moiety, and is ascribed to stabilization of mitochondrial membrane potential, induction of Bcl-2 and activation of the PKC signalling pathway (Youdim *et al.*, 2005).

Based on the abovementioned beneficial effects of TVP1022, in the present study we tested the working hypothesis that this compound would provide cardioprotection in the rat I/R model. In order to reproduce the clinical settings of acute myocardial infarction followed by reperfusion therapy, we employed a model of left anterior descending (LAD) artery occlusion for 30 min followed by reperfusion (Bhindi *et al.*, 2006). In brief, our study showed that TVP1022 provided prominent cardioprotection as demonstrated by a reduction in the infarct size, attenuation of the decline in ventricular function and diminution of mitochondrial damage caused by I/R. Thus, TVP1022 is a novel cardioprotective drug with potential for clinical benefits.

Methods

Animals

All animal care and experimental procedures were according to the institutional animal ethical committee guidelines, which conform to the *Guide for the Care and Use of Laboratory Animals* published by the US National Institutes of Health (NIH Publication No. 85–23, revised 1996) (Institutional Assurance No. A5026-01) (Ethics Numbers: IL-101-10-2007 and IL-106-11-2007). We used 3-month-old male Sprague-Dawley rats, weighing 310–340 g (n = 60). The animals were maintained at the Experimental Surgical Unit of the Technion, and fed on normal rodent chow diet, with tap water *ad libitum*, and housed at a constant temperature and relative humidity under a regular light/dark schedule (12 h : 12 h). All operators including the surgeon and echocardiography technician were unaware of the treatment given to the groups.

The I/R model and drug administration

The I/R model was generated by LAD occlusion for 30 min followed by 4 h or 24 h reperfusion (Bhindi *et al.*, 2006). In brief, rats were anaesthetized with a combination of 87 mg·kg^{-1} ketamine and 13 mg·kg^{-1} xylazine, intubated, mechanically ventilated at a rate of 80–90 cycles·min^{-1} with a tidal volume of 1–2 mL·100 g^{-1}, and the surgical procedures performed as previously described (Bhindi *et al.*, 2006). For the 24 h reperfusion protocol, TVP1022 (20 or 40 mg·kg^{-1}) dissolved in saline or vehicle was administered in two consecutive doses: (i) an i.v. dose 5 min before reperfusion, in order to achieve, rapidly, therapeutic blood levels in the anaesthetized animal; (ii) a p.o. dose 4 h after reperfusion. For the 4 h reperfusion protocol, TVP1022 (40 mg·kg^{-1} I.V) or vehicle was administered once, 5 min before reperfusion. Altogether, 16 rats were analysed at 4 h and 31 rats were analysed at 24 h of reperfusion. An overall mortality rate of 27% was observed during the surgical procedure and 24 h thereafter.

Determination of the viable area, area at risk and infarct size

The viable area, area at risk (AAR) and infarct size were determined using the triphenyltetrazolium chloride (TTC) staining (Reinhardt *et al.*, 1993; Ojha *et al.*, 2008). After *in vivo* staining with Evan's blue, the heart was removed, transferred to –80°C for 5–6 min and cut manually into seven to nine transverse slices. The slices were dipped in 1% TTC solution (in double-distilled water pH = 7.4) at 37°C for 20 min, rinsed in phosphate-buffered saline (PBS) and weighed. Improvement of colour delineation was achieved by keeping the slices for 3 weeks in a preservative solution of PBS + sodium azide (0.01%) at 4°C (Pitts *et al.*, 2007). Subsequently, the slices were placed on a light table and photographed on both sides. Using the ImageJ software (NIH, Boston, MA, USA http://rsb.info.nih.gov/ij), the pictures were analysed and the different areas were delineated. Using the weights of the slices and the percentages of the different coloured areas, the percent of viable cardiac muscle (dark blue), AAR (red and white) and infarcted area (white) of the left ventricle (LV) were calculated. The analysis included rats with AAR >20%.

Echocardiographic measurements

For the echocardiographic measurements, rats were lightly sedated by an intraperitoneal injection of a sub-anaesthetic dose of 29 mg·kg^{-1} ketamine plus 4.3 mg·kg^{-1} xylazine (Liu *et al.*, 2006; Stein *et al.*, 2007). After sedation, the rats were placed in a left lateral decubitus position and scanned via a commercially available echo-scanner – Vivid™ *i* ultrasound cardiovascular system (GE Healthcare Inc., Haifa, Israel) using a 10S phased array paediatric transducer and a cardiac application. The transmission frequency was 10 MHz, the depth was 2.5 cm and the frame rate was 225 frames·s^{-1}. The measurements included three parasternal short axis sections: at the mitral valve, papillary muscle (PM) and apex (AP) levels.

For each rat, two measurements were performed: before (baseline) LAD occlusion and after 24 h of reperfusion. To assess ventricular function, two parameters were employed: (i) ejection fraction (EF) (cardiac output/LV diastolic volume) was determined by the Vivid *i* LV function software; (ii) fractional shortening (FS) which takes into consideration one 2D cross-section of the heart. Specifically, in the M-mode records, the LV intraventricular diameters (LVID) were measured at systole and diastole (LVIDs and LVIDd, respectively), and FS was calculated as follows: $FS = \frac{LVIDd - LVIDs}{LVIDd}$.

Speckle tracking echocardiography (STE)

The ultrasound records were post-processed by the STE program (EchoPAC Dimension '08, GE Healthcare Inc., Horten, Norway), which tracks myocardial movement and calculates LV circumferential strain (% from the diastolic state) (Rappaport *et al.*, 2006; Popovic *et al.*, 2007). We chose to use the circumferential strain parameter as it correctly identifies segmental wall motion in the rat (Popovic *et al.*, 2007). Further, circumferential strain is considered a more sensitive measure than EF because it is calculated at two different levels of the heart (PM and AP) using multiple points on the cardiac wall circumference (Rappaport *et al.*, 2006).

Isolation of mitochondria

Cardiac mitochondria were isolated from the left ventricular free wall of non-operated rats, or from the AAR 4 h after starting reperfusion, by differential centrifugation (Baines *et al.*, 2002; Argaud *et al.*, 2005). Briefly, cardiac samples were homogenized in a buffer containing (in mM): 10 HEPES, 200 mannitol, 70 sucrose, 1 EGTA and 0.25 mg·mL^{-1} trypsin. The homogenates were centrifuged at 1000× *g* for 10 min to remove nuclei and debris. The supernatant was centrifuged at 11 000× *g* for 10 min. The pellet corresponding to the mitochondrial fraction was resuspended in a swelling buffer containing (in mM): 120 KCl, 10 Tris–HCl pH 7.4, 5 KH_2PO_4 and 20 MOPS to a final concentration of 0.3 mg·mL^{-1}. Mitochondria were kept on ice and used within 1 h after isolation. Total mitochondrial protein was quantified using the Bradford assay.

Mitochondrial swelling assay

Mitochondrial swelling was assessed spectrophotometrically as a decrease in absorbance of the mitochondrial suspension, measured at 520 nm after exposure to 200 μM Ca^{2+} (Wang *et al.*, 2005). The results were presented relative to the baseline absorbance at 520 nm, just before exposing the mitochondria to high Ca^{2+}.

Cell cultures

Rat heart-derived H9c2 cells were purchased from American Type Culture Collection (Manassas, VA, USA) and cultured as previously described (Youn *et al.*, 2005). NRVM cultures were prepared from ventricles of 1 to 2-day-old Sprague-Dawley rats (Kleiner *et al.*, 2008).

The serum starvation protocol in NRVM

To induce apoptosis NRVM were incubated in serum-free medium (0% serum) for 24 h. TVP1022 (20 μM) was added to the culture medium 24 h before inducing serum starvation and was present throughout the apoptosis-inducing protocol (Kleiner *et al.*, 2008).

Induction of oxidative stress in H9c2 cardiomyoblasts

H9c2 cells were maintained in Dulbecco's modified Eagle's medium with 4.5 g·mL^{-1} glucose, 10% fetal bovine serum, 2 mM glutamine, 100 units·mL^{-1} penicillin and 100 μg·mL^{-1} streptomycin. The cells were grown (1×10^4 per well) in a 96-well plate and cultured for 24 h before the actual experiment. The cultures were treated for 24 h with TVP1022 (20 μM) before exposing the cultures to H_2O_2 for 1 h (Winstead *et al.*, 2005).

Cell viability assay

Cell viability was measured using the 3-(4.5-dimethylthiazol-2-yl)-2.5-diphenyltetrazolium (MTT) assay (Weinreb *et al.*, 2008). Briefly, at the end of the experimental protocol, the medium was replaced with a fresh medium (100 μL per well), and 5 mg·mL^{-1} of MTT solution in PBS was added to each well. After incubation at 37°C for 2 h, 100 μL of 10% SDS in 0.01N HCl were added, and the solution was mixed thoroughly and incubated for an additional 24 h. Absorption was determined in an Eliza-Reader, as the ratio of 570–650 nm signal. Cell viability was expressed as a percentage of control, untreated cells.

Apoptosis staining was performed using an *in situ* cell death detection, terminal deoxynucleotidyl transferase-mediated deoxyuridine triphosphate-digoxigenin nick end labeling (TUNEL) kit (Roche, Penzberg, Germany) according to the manufacturer's instructions. Confocal image stacks were captured with a Zeiss LSM-5, Axiovert 200 microscope, using LSM 5 analysis software (Zeiss, Oberkochen, Germany). Absolute values of 5–10 separate fields were averaged, and apoptotic cells were expressed as percentage of total cells (70–100 cells counted in each field) in three independent experiments.

Immunofluorescence analysis

H9c2 cells plated on cover slips were incubated with 50 nM MitoTracker Red (Invitrogen Co., Carlsbad, CA, USA), fixed and permeabilized, and further incubated with mouse monoclonal anti-cytochrome *c* and Cy2 goat anti-mouse. Nuclei were stained with Topro-3 (Molecular Probes, Eugene, OR, USA). The co-localization of cytochrome *c* and the MitoTracker signal was represented by the orange fluorescence. The co-localization percentage was calculated as the orange-coloured area out of the total cell area. The co-localization was analysed in five fields of each treatment sample by means of the LSM-5 software. No fluorescence was detected in the absence of the primary antibody.

Western blot analysis

Lysates were prepared from H9c2 cells or NRVM (Kleiner *et al.*, 2008; Berdichevski *et al.*, 2010), and protein concentration was determined by the Bradford assay. Equal amounts of protein from cell lysates were electrophoretically separated by sodium dodecyl sulfate-polyacrylamide gel electrophoresis and processed by standard methods (Kleiner *et al.*, 2008).

Quantification of the results was accomplished by measuring the optical density of the labelled bands from the autoradiograms, using the computerized imaging program Bio-1D (Vilber Lourmat Biotech. Bioprof, Mame La Vallee Cedex, France).

Assessment of the mitochondrial membrane potential

Mitochondrial membrane potential ($\Delta\Psi m$) was determined using the fluorescent probe 5,5′,6,6′-tetrachloro-1,1′,3,3′-tetraethyl-benzimidazolylcarbocyanine iodide (JC-1) kit (ImmunoChemistry Tech, Bloomington, MN, USA) and visualized with a fluorescence microscope (Olympus, Tokyo, Japan) with excitation at 490 nm and emission at 520 nm. The fluorescence intensity of the red/green ratio was determined using ImageJ software, and 6–10 fields were counted for each treatment sample. A decrease or increase in this ratio was interpreted as a loss or gain in $\Delta\Psi m$, respectively.

Statistical analysis

The results are presented as mean ± SEM. To compare between groups of a certain protocol, one-way ANOVA was used. To compare between parameters at different time points, two-way ANOVA was used. The Holm–Sidak test was used as the *post hoc* test whenever a significant difference was found by ANOVA. $P < 0.05$ was considered statistically significant. The analysis was performed by the SigmaStat for windows version 3.11 (Systat Software, Inc. San Jose, CA, USA).

Materials

TVP1022 was kindly donated by TEVA (Netanya, Israel). β-tubulin and β-actin antibodies, H_2O_2, 12-myristate 13-acetate (PMA), the phosphoinositide 3 kinase (PI3K) inhibitor LY294002 and the PKC inhibitor chelerythrine were purchased from Sigma Chemical Co. (St. Louis, MO, USA). The PKC inhibitor GF109203X was purchased from Calbiochem (La Jolla, CA, USA). Lab-Tek Chamber Slide system and culture plates were purchased from Nalge Nunc International (Rochester, NY, USA), mounting medium for fluorescence with 4′,6-diamidino-2-phenylindole from Vector Laboratories Inc. (Burlingame, CA, USA), electrophoresis reagents from Invitrogen Corporation (Carlsbad, CA, USA) and cell culture reagents from Biological Industries (Beth-Haemek, Israel). Phospho PKC (pan) antibody which detects PKCα, β1, β2, ζ, ε, η and δ isoforms (Alexander *et al.*, 2009), phosphoglycogen synthase kinase 3β (GSK-3β) Ser9 antibody, caspase 9 and 3 antibodies were purchased from Cell Signaling (Beverly, MA, USA). Mouse anti-cytochrome *c* and Bcl-2 antibodies were purchased from BD Biosciences Pharmingen (Oakville, Canada), and the secondary antibodies Cy2 anti-mouse/goat, monoclonal anti-mouse and polyclonal anti-rabbit were purchased from Jackson Immunoresearch Laboratories (West Grove, PA, USA). The drug and molecular target nomenclature conforms to the BJP's *Guide to Receptors and Channels* (Alexander *et al.*, 2009).

Results

TVP1022 reduced the infarct size in I/R rats

The cardioprotective efficacy of TVP1022 was demonstrated by its ability to cause a marked decrease in the infarct size, as depicted by representative ventricular sections (Figure 1A) and the summary of these experiments (Figure 1C). Specifically, while there was no difference in the AAR (% of LV) between the saline-treated rats (control) and TVP1022-treated rats (Figure 1B), the infarct size (% of AAR) was reduced ($P < 0.05$) in the TVP1022 (20 and 40 $mg \cdot kg^{-1}$) groups, providing a ~70% reduction in the infarct size, normalized to the AAR (Figure 1C).

TVP1022 attenuated the decline in ventricular function in I/R rats

In agreement with previous studies (Homes *et al.*, 1994; Onai *et al.*, 2004), at 24 h reperfusion I/R was associated with a pronounced reduction in LV function, represented by FS, EF and circumferential strain. As shown by the representative echocardiographic M-mode records (Figure 2A), whereas in the saline-treated rat, ventricular wall motion was attenuated 24 h post-I/R, the motion was relatively preserved in the TVP1022 (40 $mg \cdot kg^{-1}$)-treated rat. The summary of these experiments demonstrates that, in the saline and 20 $mg \cdot kg^{-1}$ TVP1022 groups, EF and FS decreased (albeit to a different extent) 24 h post-I/R, compared with their respective baseline levels ($P < 0.05$) (Figure 2B,C). In contrast, in the group treated with 40 $mg \cdot kg^{-1}$ TVP1022, EF and FS were not different at 24 h post-I/R, compared with baseline values, indicating that this dose of TVP1022 had attenuated the decline in ventricular function. The mean ± SEM heart rate during the echocardiographic measurements was 274 ± 3 $beats \cdot min^{-1}$ ($n = 31$).

Ventricular function was further assessed by measuring circumferential strain which represents ventricular contraction (Rappaport *et al.*, 2006). Figure 3A depicts baseline and 24 h post-I/R representative apical B-mode records for saline and TVP1022 (40 $mg \cdot kg^{-1}$)-treated rats. On each record a coloured circumferential strain map is superimposed, demonstrating the strain distribution along the cardiac wall; dark blue colours represent extreme (~ –20% to –30%) circumferential strain and lighter colours represent moderate (~0% to –10%) circumferential strain. As shown in Figure 3A, the dark blue colours, which characterize the baseline readings at all levels, were disrupted by the I/R procedure, and turned into light blue and turquoise colours. In contrast, TVP1022 (40 $mg \cdot kg^{-1}$) preserved the baseline circumferential strain pattern 24 h post-I/R. In summary (Figure 3B,C) and in agreement with the EF and FS findings, although circumferential strain was reduced ($P < 0.05$) at both the AP and PM levels in the saline and the 20 $mg \cdot kg^{-1}$ TVP1022 groups, compared with baseline, this parameter was not significantly diminished in the rats treated with 40 $mg \cdot kg^{-1}$ TVP1022. It should be noted that as the ligation was located just above the PM level, circumferential strain at this level was less affected (26%) than at lower ventricular locations, such as the AP (34%).

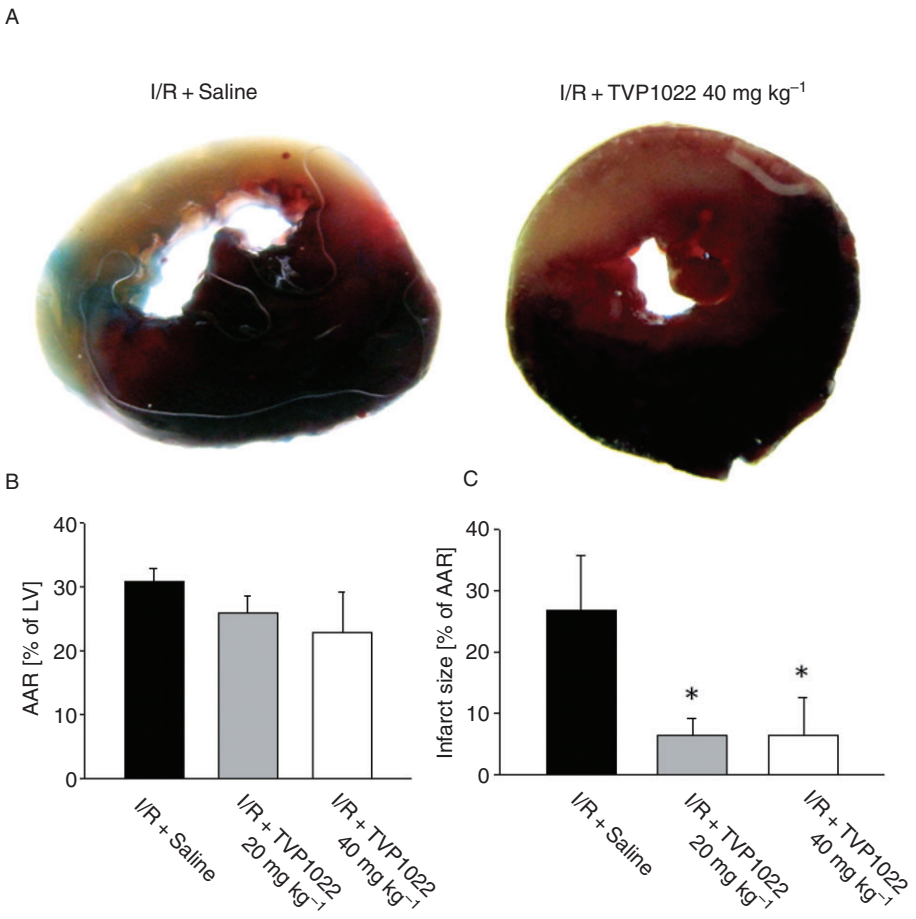

Figure 1

TVP1022 reduced the infarct size in ischaemia and reperfusion (I/R) rats. (A) Representative pictures of ventricular slices from rats treated with saline or TVP1022 (40 mg·kg^{-1}) as described in Methods. The area at risk (AAR) and infarct regions were determined at 24 h after reperfusion. Dark stain – viable area; pale stain – area at risk (AAR). (B) The AAR normalized to LV area (%). (C) The infarct size normalized to the AAR (%). Each bar represents the mean ± SEM of the I/R + saline (n = 13), I/R + TVP1022, 20 mg·kg^{-1} (n = 12) and MI + TVP1022, 40 mg·kg^{-1} (n = 6) groups. *P < 0.05 versus control.

TVP1022 prevented I/R-induced mitochondrial damage

Because mitochondria are intimately involved in I/R apoptotic damage as well as constitute a novel target for myocardial protection (Molavi and Mehta, 2004), we investigated the ability of TVP1022 to preserve mitochondrial integrity in ventricular tissue from I/R rats. Integrity was assessed by determining Ca^{2+}-induced mitochondrial swelling (Borillo *et al.*, 2010) measured as a decrease in 520 nm wavelength (A_{520}) readout in isolated mitochondria from control (see details in Methods), I/R + saline and I/R + TVP1022-treated rats. Figure 4 shows that in mitochondria isolated from intact rats, high Ca^{2+} decreased the A_{520} signal in the course of 5 min. In contrast, in mitochondria isolated from the AAR of saline-treated I/R rats, the A_{520} signal was only slightly decreased, presumably because these mitochondria were already considerably swollen due to the I/R insult. However, in mitochondria isolated from the AAR of the I/R + TVP1022 group, the swelling response was much more pronounced than in the I/R + saline group (P < 0.001), resembling the response of mitochondria from samples of intact myocardium.

In vitro effects of TVP1022 on heart-derived cells

In order to determine the protective efficacy of TVP1022 *in vitro* under ischaemic and oxidative stress conditions which simulate key components of the I/R insult, we used two common models in NRVM cultures: serum starvation, and exposure to H_2O_2 which is a potent reactive oxygen species (ROS)-inducing cardiac cell death. In the first stage of these experiments, NRVM were grown in serum-free medium in the absence or presence of TVP1022. The apoptosis-inducing capacity of serum starvation is reflected by the increase in apoptotic cells, compared with those cultured in full serum, demonstrated by the representative pictures and by the summary of these experiments (Figure 5A). In agreement with its known anti-apoptotic efficacy and with our previous

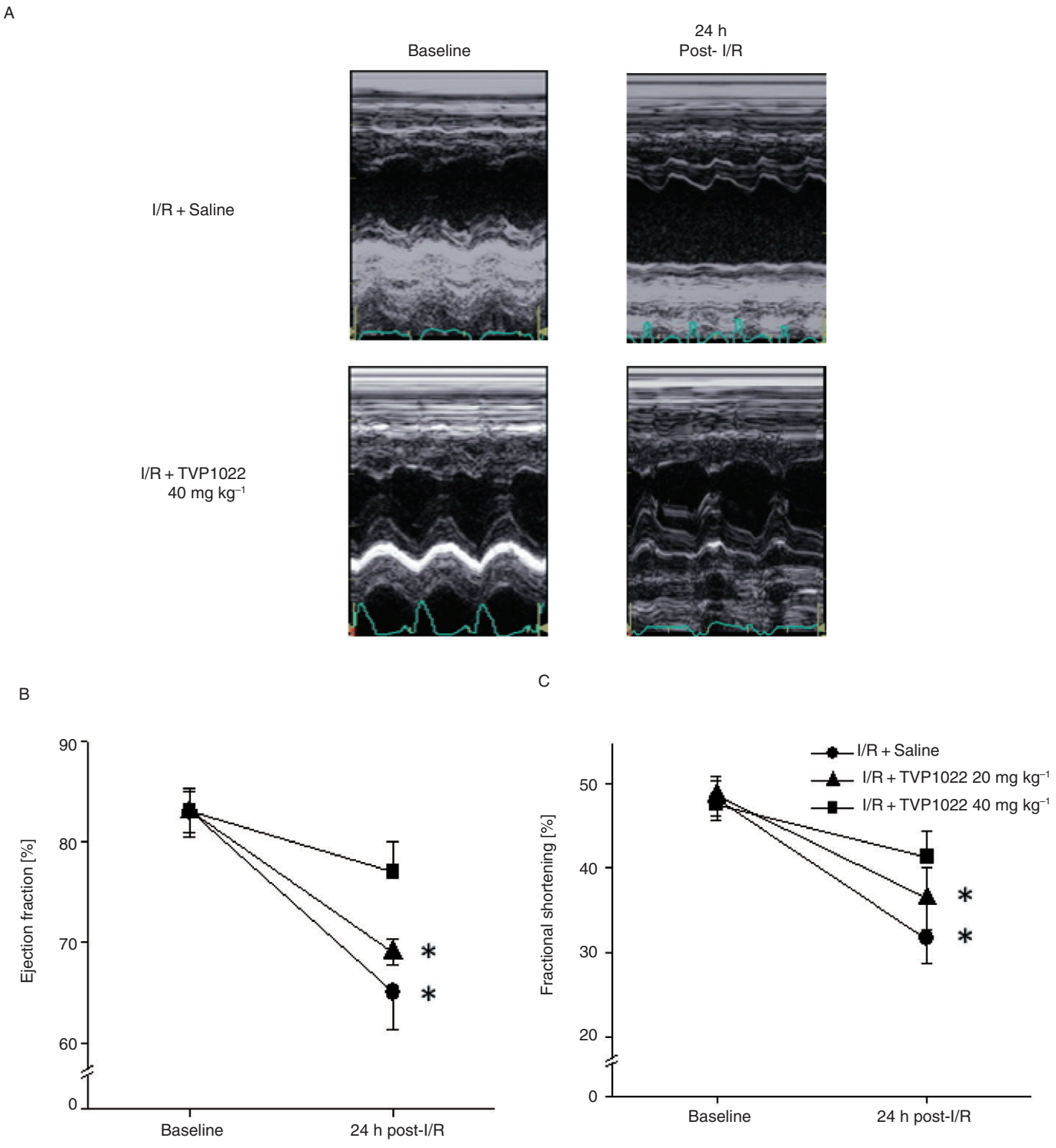

Figure 2

TVP1022 attenuated the decline in ventricular function in ischaemia and reperfusion (I/R rats). (A) Representative echocardiographic 2D-mode records obtained at the papillary muscle level at baseline and 24 h post-I/R, in rats treated with saline (upper panel) or TVP1022 40 mg·kg^{-1} (lower panel). (B) Ejection fraction and (C) fractional shortening measured at baseline and 24 h post-I/R in the different groups: I/R + Saline (n = 10), I/R + TVP1022, 20 mg·kg^{-1} (n = 9) and I/R + TVP1022, 40 mg·kg^{-1} (n = 10). *P < 0.05. versus baseline measurement.

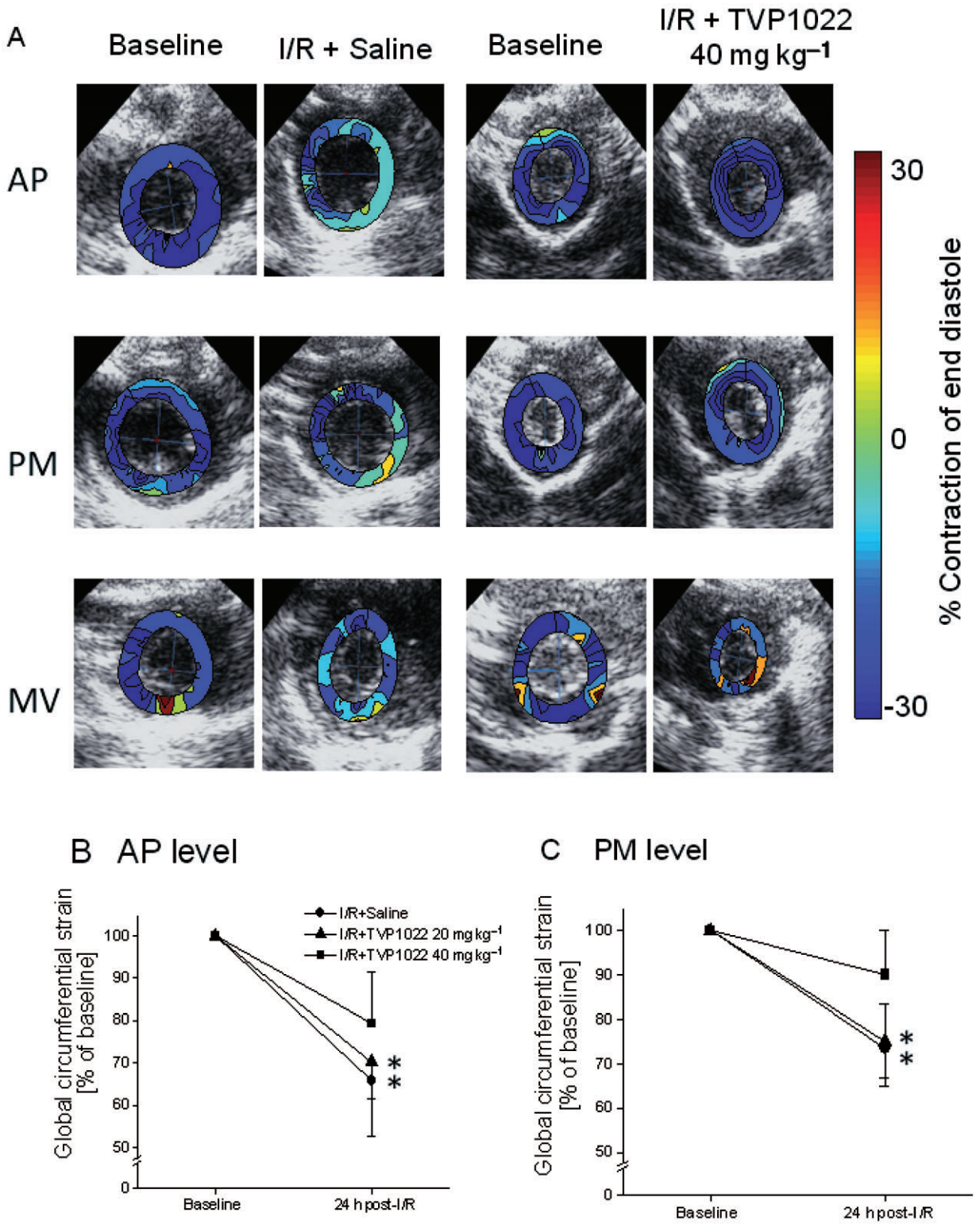

Figure 3

TVP1022 preserved global circumferential strain 24 h post-ischaemia and reperfusion (I/R). (A) Two sets of representative circumferential strain maps (coloured circles) implanted on the echocardiographic records. Each set includes baseline and 24 h post-I/R records of three B-mode short-axis records. Upper panel – apex (AP); middle panel – papillary muscle (PM); lower panel – mitral valve (MV). Negative circumferential strain (blue) indicates myocardial contraction. (B) AP and (C) PM circumferential strain measured at baseline and 24 h post-I/R. Results were expressed as mean ± SEM obtained from the I/R + saline ($n = 16$), TVP1022 20 mg·kg^{-1} ($n = 14$) and TVP1022 40 mg·kg^{-1} ($n = 9$) groups. *$P < 0.05$ versus baseline measurement.

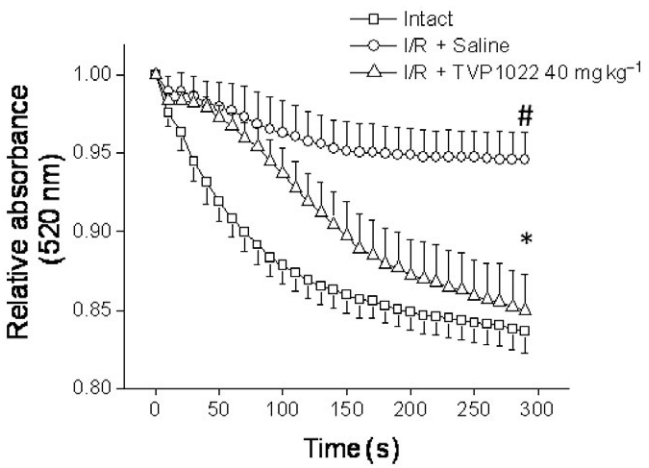

Figure 4

TVP1022 attenuated ischaemia and reperfusion (I/R)-induced mitochondrial damage. Mitochondria were isolated from intact ventricular tissue ($n = 5$), and from the area at risk from I/R + saline ($n = 5$) and I/R + TVP1022 40 mg·kg^{-1} ($n = 6$) groups. The absorbance at 520 nm of isolated mitochondria was recorded every 10 s for 5 min after the addition of 200 μM Ca^{2+}. The relative absorbance is presented as mean ± SEM. #$P < 0.001$ versus intact; *$P < 0.001$ versus I/R + saline.

report (Kleiner *et al.*, 2008), TVP1022 (20 μM) decreased ($P < 0.05$) the number of apoptotic NRVM (Figure 5A). Consistent with its anti-apoptotic effect, TVP1022 attenuated the expression of the cleaved, activated forms of caspases 9 and 3 (46 ± 1% and 43 ± 7%, respectively, $n = 3$, $P < 0.05$ versus serum-free medium). In addition, TVP1022 attenuated the decrease in the levels of the pro-survival protein Bcl-2 (2.05 ± 0.2 fold, $n = 3$, $P < 0.05$ versus serum free) (Figure 5B).

In addition to NRVM, we utilized H9c2 rat-derived cardiomyoblasts which are commonly used for investigating death/survival signalling pathways in cardiac cells (Winstead *et al.*, 2005). As H_2O_2 induces a similar oxidative stress in H9c2 cells and in NRVM, the former source constitutes a useful model for investigating oxidative stress-induced injury to cardiac cells (Chen *et al.*, 2001; Sheng *et al.*, 2010). As shown in Figure 6A, TVP1022 dose dependently increased cell viability of H9c2 cells exposed to H_2O_2 (300 μM). In control experiments TVP1022 alone did not affect cell viability (data not shown). As oxidative stress facilitates the mitochondrial permeability transition pore (MPTP) opening, thereby depolarizing ΔΨm which leads to the release of apoptogenic proteins into the cytoplasm, we determined the ability of TVP1022 (10 μM) to alleviate H_2O_2-induced decrease in ΔΨm. As demonstrated in Figure 6B, control untreated H9c2 cells exhibit many brightly stained mitochondria-emitting red fluorescence spots, indicative of normal uptake of dye into mitochondria driven by fully polarized ΔΨm. In contrast, H9c2 cells exposed to H_2O_2 display fewer red spots and a diffuse pattern of green JC-1 spots scattered in the cytoplasm, suggesting a reduction in ΔΨm. In contrast, H9c2 cells treated with TVP1022 showed a smaller decrease in the red fluorescence, likely to result from a partial preservation of ΔΨm. In summary, an analysis of four independent experiments showed that ΔΨm (expressed as the ratio of red/green fluorescence intensity) of H9c2 cells exposed to H_2O_2 was 24 ± 1% of the control value ($P < 0.05$), while in TVP1022-treated cells, the ratio was 38 ± 3% ($P < 0.05$ versus H_2O_2 alone).

For further support of our findings, we determined the ability of TVP1022 to inhibit H_2O_2-induced release of cytochrome *c* from the mitochondria by assessing the co-localization between the fluorescence signals of cytochrome *c* and the MitoTracker fluorescence-labelled mitochondria (Figure 6C). Whereas H_2O_2 (300 μM) increased the release of cytochrome *c* from the mitochondria, indicated by the increment in the green fluorescence distribution and decreased orange fluorescence in the merged panel, in the presence of TVP1022, this phenomenon was attenuated. As summarized in Figure 6C, TVP1022 diminished the decline in the co-localization of cytochrome *c* and mitochondria caused by H_2O_2, suggesting that the drug maintained mitochondrial integrity.

PKC and PI3K/AKT/GSK-3β signalling pathways are involved in TVP1022 cardioprotection

In this series of experiments we tested the hypothesis that the PKC and PI3K/AKT/GSK-3β pathways underlie the cardioprotective efficacy of TVP1022. Figure 7 shows that chelerythrine (a specific PKC inhibitor) and LY294002 (a PI3K inhibitor) blocked the cytoprotective effect of TVP1022 in H9c2 cells exposed to H_2O_2 (Figure 7A). Further supporting data are the findings that incubating H9c2 cells with TVP1022 for 30 min dose dependently increased phospho-PKC levels, similar to the effect of the PKC activator PMA (Figure 7B). Importantly, this increase in phospho-PKC level by TVP1022 was blocked by pre-incubation with chelerythrine (5 μM) (Figure 7C). Additionally, TVP1022 dose dependently increased GSK-3β (Ser9) phosphorylation (Figure 7D); this effect was attenuated by pre-incubation with LY294002 (10 μM) and GF109203X (2.5 μM), which inhibit GSK-3β phosphorylation (Figure 7E). Collectively, these findings suggest that both PKC and PI3K/AKT/GSK-3β signalling pathways are involved in the anti-apoptotic effect of TVP1022. These findings in H9c2 cells were further supported in NRVM by demonstrating that TVP1022 increased PKC and GSK-3β (Ser9) phosphorylation (Figure 8A,C) and that these effects were blocked by pre-incubation with chelerythrine (5 μM) and LY294002 (10 μM) (Figure 8B,D).

Discussion

The present study showed that TVP1022 exerted a protective effect against I/R injury in the rat heart and attenuated oxidative stress *in vitro* via PKC and GSK-3β signalling pathways. The major findings were: (i) pre-reperfusion followed by post-reperfusion administration of TVP1022 reduced the infarct size and attenuated the decline in ventricular function; (ii) TVP1022 preserved the mitochondrial integrity in the AAR; (iii) *in vitro*, TVP1022 conferred cytoprotection in serum-free and H_2O_2-induced apoptotic models; (iv) TVP1022 caused phosphorylation of both PKC and GSK-3β. Collectively, these

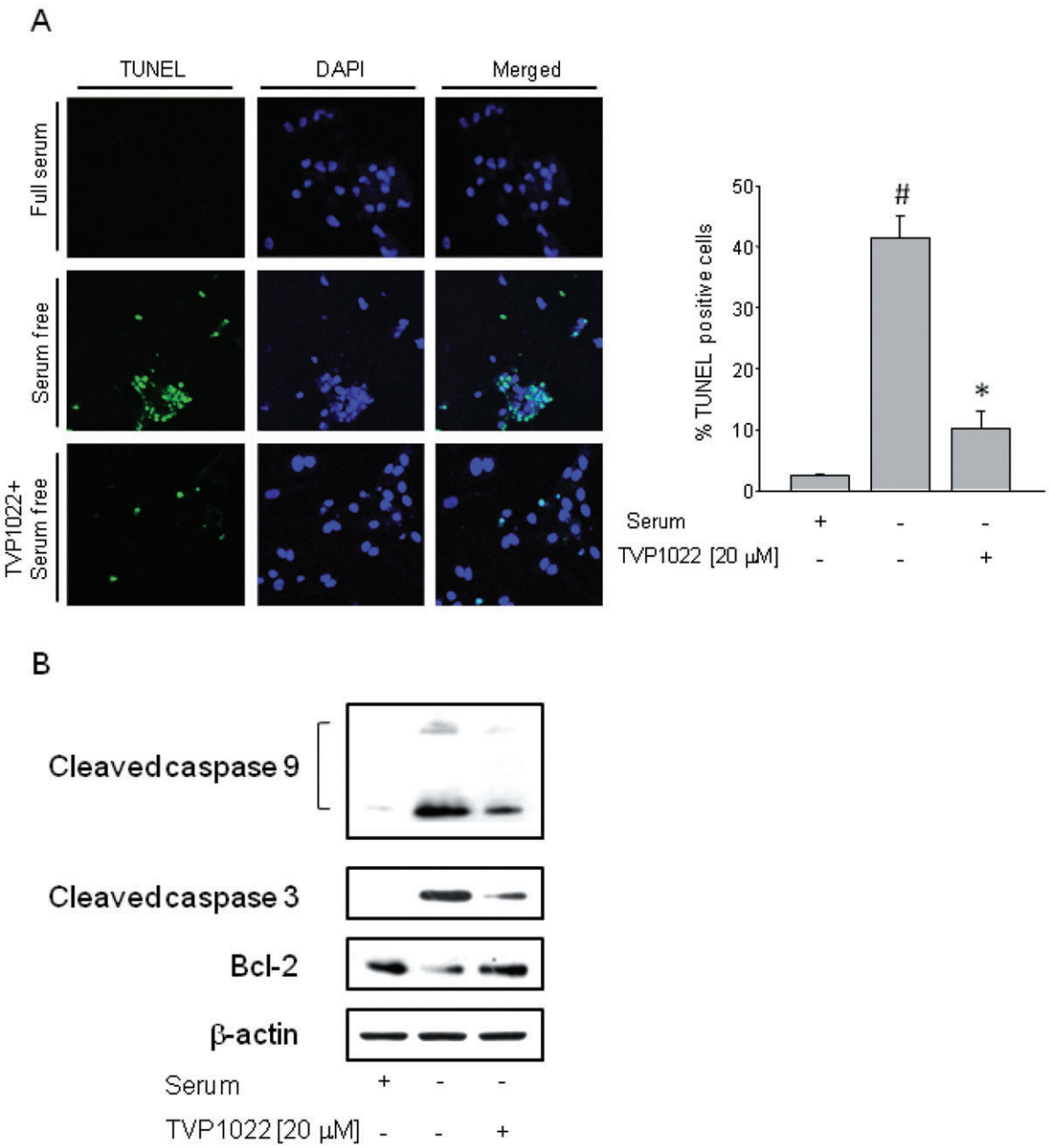

Figure 5

TVP1022 protected neonatal rat ventricular myocytes (NRVM) against serum starvation-induced apoptosis. NRVM were incubated with or without TVP1022 in serum free medium. (A) Apoptotic nuclei were identified by TUNEL analysis. Absolute values of 5–10 separate fields were averaged, and apoptotic cells were expressed as percentage of total cells in three independent experiments. #$P < 0.05$ versus full serum; *$P < 0.05$ versus serum-free medium. (B) Representative Western blots of cleaved caspase 9, cleaved caspase 3 and Bcl-2. Equal loading was checked with an antibody against β-actin ($n = 3$). DAPI, 4′,6-diamidino-2-phenylindole; TUNEL, terminal deoxynucleotidyl transferase-mediated deoxyuridine triphosphate-digoxigenin nick end labeling.

findings demonstrate that TVP1022 provides significant protection against cardiac I/R injury.

TVP1022 protects the myocardium in the rat I/R model

The clinical setting simulated by the current experimental protocol is of a patient diagnosed with myocardial infarction, and treated with a cardioprotective drug prior to and following reperfusion therapy. Hence, the I/R procedure resulted in an AAR of about 27% of the LV, of which about one-third was infarcted tissue. Under these experimental conditions, both 20 and 40 mg·kg^{-1} TVP1022, given 5 min before reperfusion and 4 h thereafter, reduced the infarct size (normalized to AAR) by ~70%. In patients, a similar or even a smaller reduction in infarct size will have a remarkable beneficial effect on

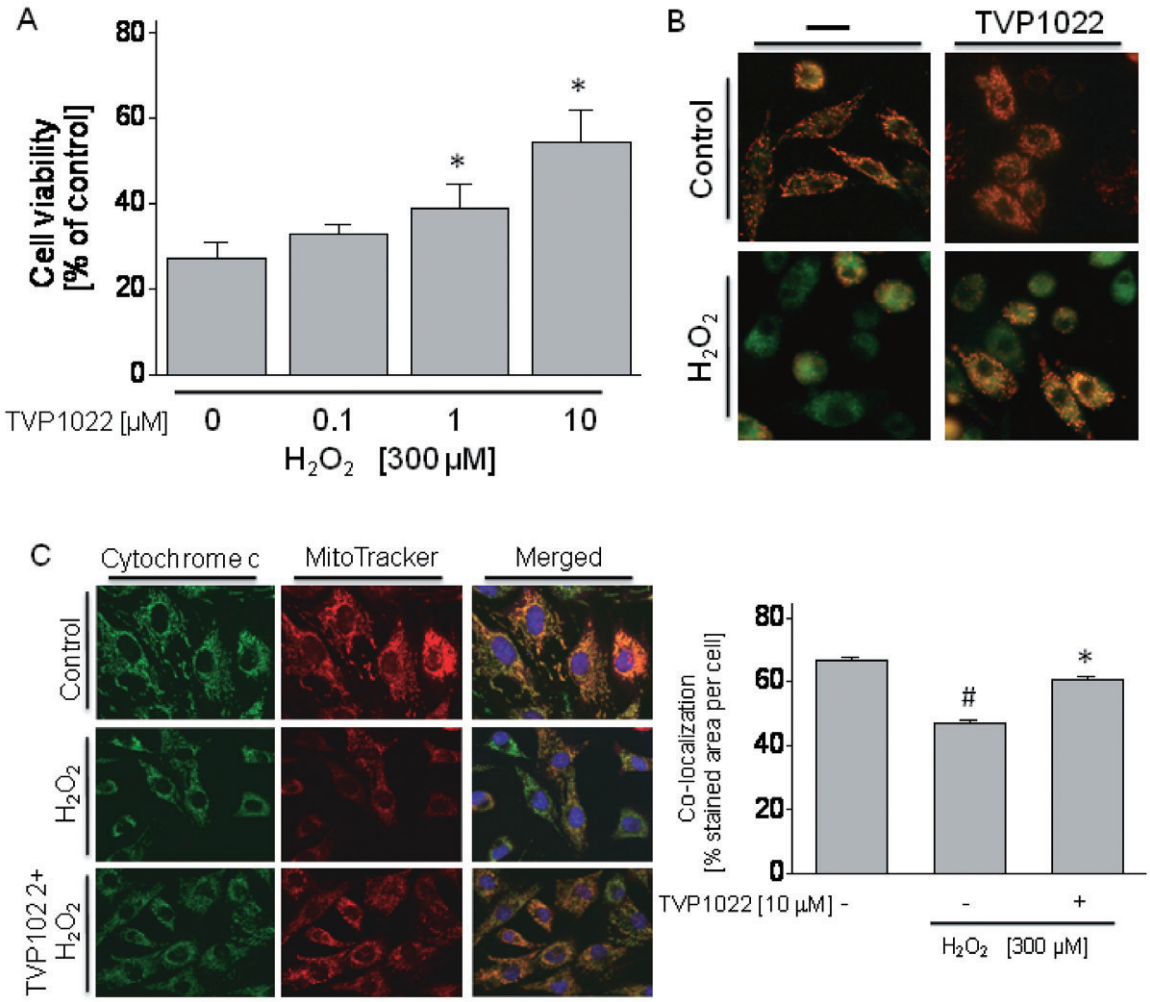

Figure 6

TVP1022 protected H9c2 cells from H_2O_2-induced cardiotoxicity. H9c2 cells were treated with H_2O_2 (300 μM) in the absence or presence of TVP1022 (0.1, 1 and 10 μM) for 1 h. (A) Cell viability was measured using the MTT assay. (B) Representative images of H9c2 cells stained with JC-1. (C) Representative immunofluorescence images of cytochrome *c* and a quantitative summary of four independent experiments. Cytochrome *c* (green); mitochondrial staining with MitoTracker (red); nuclear staining with Topro (blue) and merged images of cytochrome *c* and mitochondrial staining showing co-localization in yellow. Co-localization is presented as percentage of stained area per total cell area (n = 20–30 cells). #P < 0.05 versus control; *P < 0.05 versus H_2O_2. MTT, 3-(4.5-dimethylthiazol-2-yl)-2.5-diphenyltetrazolium.

morbidity and mortality following a myocardial infarction. Further, TVP1022 (40 mg·kg^{-1}) diminished the decrease in EF, FS and circumferential strain at the PM and AP levels, 24 h post-I/R. An observation unaccounted for in the current study is that whereas both 20 and 40 mg·kg^{-1} TVP1022 reduced infarct size similarly, the beneficial effect of 40 mg·kg^{-1} on ventricular function was more pronounced than that of 20 mg·kg^{-1}.

As mitochondria are key elements in I/R injury, we assessed the mitochondrial functional integrity by measuring their swelling response to high Ca^{2+} concentration (Crompton, 1999; Wang *et al.*, 2005). In agreement with its ability to reduce infarct size and preserve LV function, treating I/R rats with one dose of TVP1022 5 min before reperfusion improved the mitochondrial swelling response (of mitochondria isolated from the AAR), compared with the I/R + saline group, suggesting an improvement in mitochondrial function. These findings are in agreement with previous studies (Argaud *et al.*, 2005; Cour *et al.* 2011) showing the beneficial effect of inhibiting MPTP opening in a model of reperfusion. Specifically, in New Zealand rabbits treated with cyclosporin A or NIM811, inhibition of MPTP opening pre-reperfusion caused almost full recovery of cardiac haemodynamics.

Protective effects of TVP1022 on heart-derived cells

To determine whether TVP1022-induced cardioprotection *in vivo* was due to a direct effect on cardiomyocytes, we exposed H9c2 cells and NRVM to serum-free medium or to H_2O_2, both constituting common models of oxidative stress-induced apoptosis (simulating a key component of the I/R insult) (Umansky *et al.*, 1995; Bialik *et al.*, 1999; Bonavita *et al.*, 2003; Sheng *et al.*, 2010). H_2O_2 is an important component of the ROS, which are increased in the course of I/R injury, and

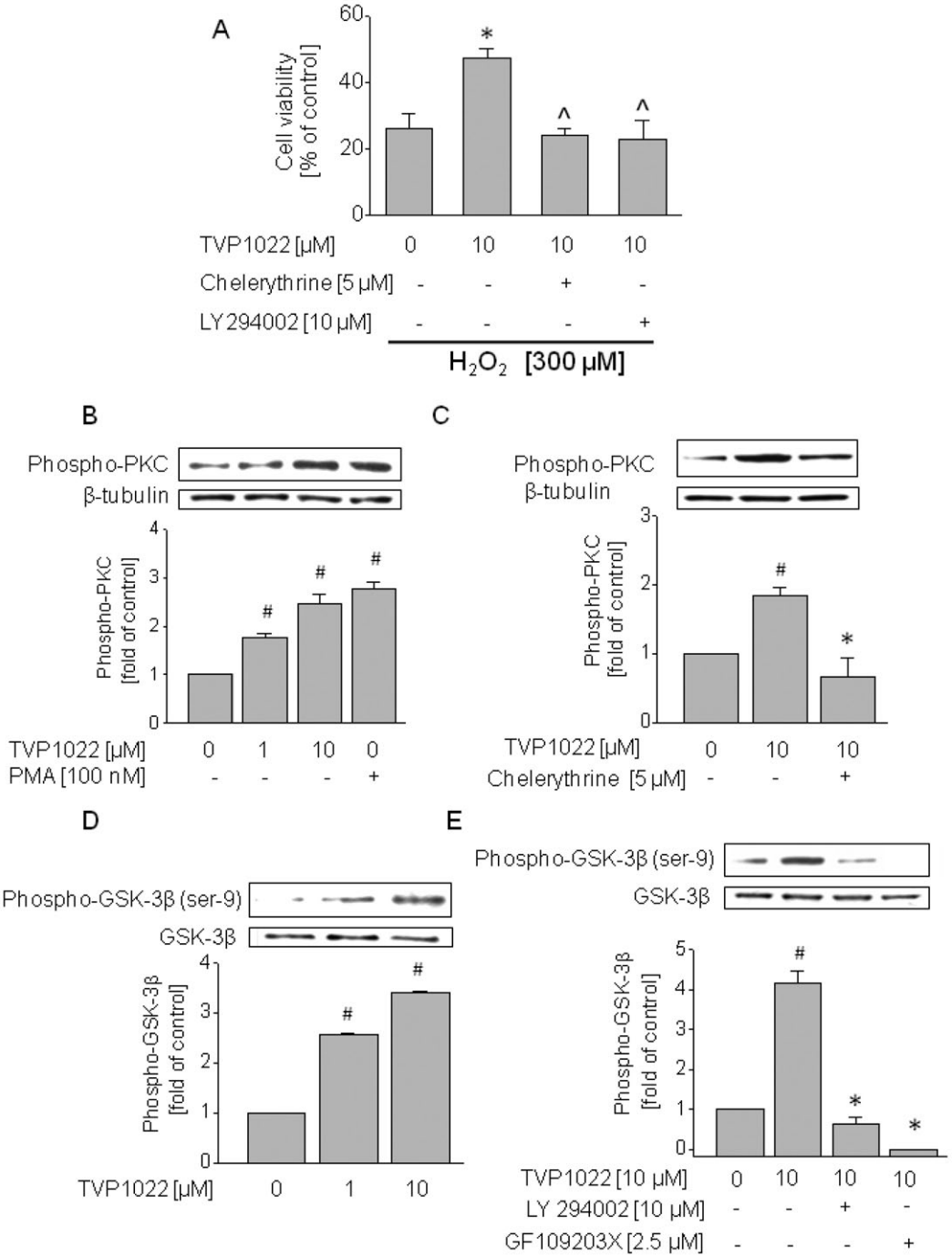

Figure 7

The involvement of the PKC/GSK-3β and PI3K/AKT pathways in the cardioprotective efficacy of TVP1022 in H9c2 cells. (A) H9c2 cells were pre-incubated without or with chelerythrine (5 μM) or LY294002 (10 μM) for 1 h, and then further incubated with H_2O_2 (300 μM) in the absence or presence of TVP1022 (10 μM) for 1 h. Cell viability was measured by the MTT assay. Results are presented as percent of control untreated cells. $n = 3$ experiments. *$P < 0.05$ versus H_2O_2 alone; ^$P < 0.05$ versus H_2O_2 + TVP1022. (B) H9c2 cells were incubated without or with TVP1022 (1 μM and 10 μM) or PMA (100 nM) for 30 min. (C) H9c2 cells were pre-incubated with a vehicle alone, or with chelerythrine (5 μM) for 1 h, and then incubated without or with TVP1022 (10 μM) for 30 min. Phosphorylated PKC levels were analysed in cell lysates and were normalized to β-tubulin levels. (D) H9c2 cells were incubated without or with TVP1022 (1 μM and 10 μM) for 30 min. (E) H9c2 cells were pre-incubated with a vehicle alone, or with LY294002 (10 μM) or GF109203X (2.5 μM), and then incubated without or with TVP1022 (10 μM) for 30 min. Phosphorylated GSK-3β (Ser9) levels were analysed in cell lysates and normalized to GSK-3β levels. In panels (B)–(E), upper lanes show representative Western blots of the respective proteins in the different experimental groups. Equal loading was checked with an antibody against β-tubulin or GSK-3β. All blots are representative of three independent experiments, summarized in bar graphs below. #$P < 0.05$ versus control untreated cells; *$P < 0.05$ versus TVP1022. MTT, 3-(4.5-dimethylthiazol-2-yl)-2.5-diphenyltetrazolium; PMA, 12-myristate 13-acetate.

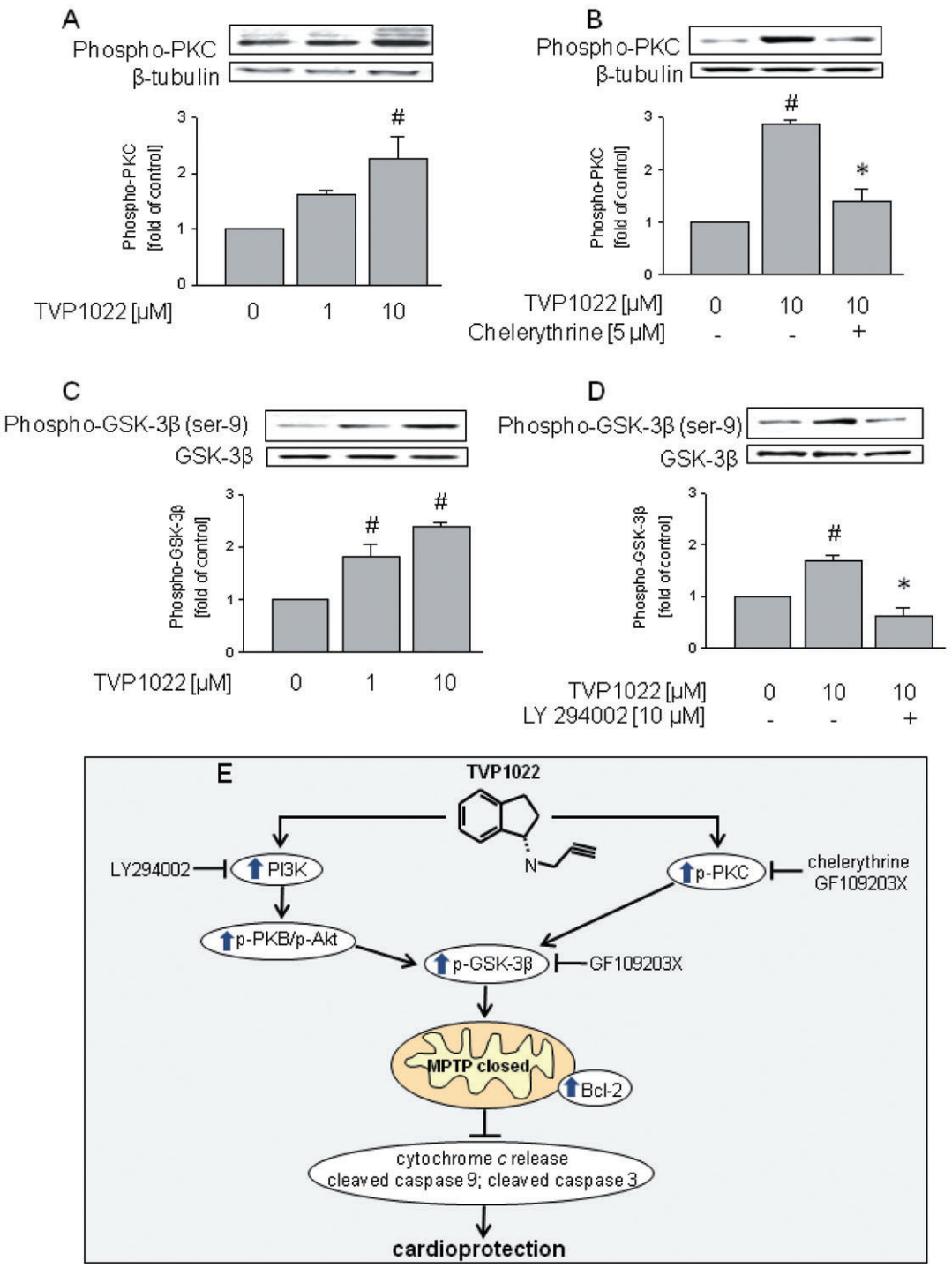

Figure 8

The effect of TVP1022 on phosphorylation of PKC and GSK-3β in neonatal rat ventricular myocytes (NRVM). NRVM were incubated without or with TVP1022 (1 or 10 μM) for 30 min. Phosphorylation levels of (A) PKC and (C) GSK-3β (Ser9) were analysed in NRVM lysates by Western blotting. NRVM were pre-incubated with vehicle alone, or with (B) chelerythrine (5 μM) or (D) LY294002 (10 μM) for 1 h, and then incubated without or with TVP1022 (10 μM) for 30 min. Phosphorylated PKC and GSK-3β levels were analysed in cell lysates and normalized to β-tubulin or to GSK-3β levels respectively. In panels (A)–(D) upper lanes show representative Western blots of the respective proteins in the different experimental groups. Equal loading was checked with an antibody against β-tubulin or GSK-3β. All blots are representative of three independent experiments, summarized in bar graphs below. #$P < 0.05$ versus control untreated cells; *$P < 0.05$ versus TVP1022. (E) A schematic model for the cardioprotective effect of TVP1022. TVP1022 inactivates GSK-3β via PKC and PI3K signalling pathways, resulting in cardioprotection against MPTP opening, and mitochondrial cytochrome *c* release into the cytosol. In turn, TVP1022 increases the levels of anti-apoptotic protein Bcl-2 and inhibits the activation of caspases 9 and 3. MPTP, mitochondrial permeability transition pore.

also contribute to the pathogenesis of heart failure (Chen *et al.*, 2001; Winstead *et al.*, 2005; Sheng *et al.*, 2010). The *in vitro* experiments demonstrated that TVP1022 attenuated serum starvation and H_2O_2-induced apoptosis. These anti-apoptotic effects were associated with the preservation of mitochondrial membrane potential and Bcl-2 levels, inhibition of mitochondrial cytochrome *c* release and of the increased levels of cleaved caspases 9 and 3. These observations are consistent with our previous study demonstrating that TVP1022 attenuated doxorubicin- and serum starvation-induced apoptosis in NRVM (Kleiner *et al.*, 2008). Several studies have shown that caspase 3 plays a central role in the execution phase of cell apoptosis (Porter and Janicke, 1999). The activation of caspase 3 is governed by a group of signalling cascades, among which the interaction of the anti-apoptotic Bcl-2 and the pro-apoptotic Bax proteins plays a critical role. It was demonstrated that Bcl-2 is capable of forming a heterodimer with Bax, thereby preventing Bax homodimerization, the release of mitochondrial cytochrome *c*, and the sequential activation of caspase 9 and caspase 3 (Narita *et al.*, 1998; Murphy *et al.*, 2000). The present findings are also in agreement with our recent studies showing that TVP1022 and its (R)-enantiomer rasagiline, exhibit similar neuroprotective activities in response to various neurotoxins in neuronal cell cultures and in an *in vivo* model of close head injury (Huang *et al.*, 1999; Youdim *et al.*, 2001; 2005). The molecular mechanisms underlying the neuroprotective effects of rasagiline were found to involve suppression of MPTP opening, prevention of cytochrome *c* release and caspase 3 activation, and nuclear glyceraldehyde-3-phosphate dehydrogenase translocation and induction of the pro-survival protein Bcl-2 (Naoi and Maruyama, 2009).

A number of intracellular signalling elements were proposed to be involved in cardioprotection against I/R injury, including PKC and AKT, which may regulate GSK-3β to promote cell survival (Juhaszova *et al.*, 2009). Previous studies have shown that GSK-3β is a putative regulator of MPTP opening, and thus several cytoprotective signals may converge on this kinase (Juhaszova *et al.*, 2004; Juhaszova *et al.*, 2009; Zorov *et al.*, 2009). Indeed, here we demonstrated that PI3K/AKT/GSK-3β inhibition blocked the cardioprotective effect of TVP1022 against apoptosis induced by oxidative stress. The present study also shows that TVP1022 dose dependently increased phospho-PKC and phospho-(Ser9) GSK-3β levels in both H9c2 cells and NRVM; these effects were attenuated by specific inhibitors of PKC and GSK-3β signalling pathways. Moreover, we previously reported that the R-enantiomer rasagiline and propargylamine increased mRNA expression levels and activation of the isoenzyme PKCε (Weinreb *et al.*, 2004; Bar-Am *et al.*, 2005). Indeed, it was clearly shown that PKCε has distinct functions in cardioprotection (Chen *et al.*, 2001; Inagaki *et al.*, 2006; Garlid *et al.*, 2009). Notably, our inhibition studies illustrated that the PKC inhibitor GF109203X also inhibited TVP1022-induced phospho-GSK-3β(Ser9) levels, in accordance with a previous finding showing that GSK-3β can be inactivated by the PKC pathway (Gross *et al.*, 2004; Juhaszova *et al.*, 2004). In this regard, an earlier study by Fang *et al.* in non-cardiac cells demonstrated that PKC induced the phosphorylation of GSK-3β(Ser9) by an AKT-independent mechanism (Fang *et al.*, 2002). Thus, PKC may be responsible for PI3K/AKT-dependent phosphorylation of GSK-3β, although the possibility of involvement of other kinases cannot be excluded.

In summary, we have demonstrated that TVP1022 attenuated H_2O_2-induced cytotoxicity in cardiac cells *in vitro* via the PKC/GSK-3β pathway. The mechanism underlying the protective efficacy appears to involve inhibition of MPTP opening, thus leading to decreased cytochrome *c* release from the mitochondria (see model scheme in Figure 8E) (Juhaszova *et al.*, 2004). As inhibiting the opening of MPTP is a critical event in the acute cardioprotection induced by pre-conditioning and post-conditioning, the current findings suggest that TVP1022 may confer cardioprotection against myocardial infarction and reperfusion by preserving mitochondrial integrity via activation of the PKC/GSK-3β pathway.

Acknowledgements

This work was supported by the Alfred Mann Institute at the Technion, The Bi-National US-Israel Foundation and the Rappaport Family Institute at the Technion.

Conflicts of interest

None.

References

Alexander S, Mathie A, Peters J (2009). Guide to receptors and channels (GRAC), 4th edn. Br J Pharmacol 158 (Suppl. 1): S1–254.

Argaud L, Gateau-Roesch O, Muntean D, Chalabreysse L, Loufouat J, Robert D *et al.* (2005). Specific inhibition of the mitochondrial permeability transition prevents lethal reperfusion injury. J Mol Cell Cardiol 38: 367–374.

Baines C, Zhang J, Wang G, Zheng Y, Xiu J, Cardwell E *et al.* (2002). Mitochondrial PKCepsilon and MAPK form signaling modules in the murine heart: enhanced mitochondrial PKCepsilon-MAPK interactions and differential MAPK activation in PKCepsilon-induced cardioprotection. Circ Res 90: 390–397.

Bar-Am O, Weinreb O, Amit T, Youdim MB (2005). Regulation of Bcl-2 family proteins, neurotrophic factors, and APP processing in the neurorescue activity of propargylamine. FASEB J 19: 1899–1901.

Berdichevski A, Meiry G, Milman F, Reiter I, Sedan O, Eliyahu S *et al.* (2010). TVP1022 protects neonatal rat ventricular myocytes against doxorubicin-induced functional derangements. J Pharmacol Exp Ther 332: 413–420.

Bhindi R, Witting P, Mcmahon A, Khachigian L, Lowe H (2006). Rat models of myocardial infarction. Pathogenetic insights and clinical relevance. Thromb Haemost 96: 602–610.

Bialik S, Cryns V, Drincic A, Miyata S, Wollowick A, Srinivasan A *et al.* (1999). The mitochondrial apoptotic pathway is activated by serum and glucose deprivation in cardiac myocytes. Circ Res 85: 403–414.

Black S (2000). *In vivo* models of myocardial ischemia and reperfusion injury: application to drug discovery and evaluation. J Pharmacol Toxicol Methods 43: 153–167.

Bonavita F, Stefanelli C, Giordano E, Columbaro M, Facchini A, Bonafe F *et al.* (2003). H9c2 cardiac myoblasts undergo apoptosis in a model of ischemia consisting of serum deprivation and hypoxia: inhibition by PMA. FEBS Lett 536: 85–91.

Borillo G, Mason M, Quijada P, Volkers M, Cottage C, Mcgregor M *et al.* (2010). Pim-1 kinase protects mitochondrial integrity in cardiomyocytes. Circ Res 106: 1265–1274.

Chen L, Hahn H, Wu G, Chen CH, Liron T, Schechtman D *et al.* (2001). Opposing cardioprotective actions and parallel hypertrophic effects of delta PKC and epsilon PKC. Proc Natl Acad Sci USA 98: 11114–11119.

Cour M, Loufouat S, Paillard M, Augeul L, Goudable J, Ovize M *et al.* (2011). Inhibition of mitochondrial permeability transition to prevent the post-cardiac arrest syndrome: a pre-clinical study. Eur Heart J 32: 226–235.

Crompton M (1999). The mitochondrial permeability transition pore and its role in cell death. Biochem J 341: 233–249.

Downey J, Cohen M (2009). Why do we still not have cardioprotective drugs? Circ J 73: 1171–1177.

Fang X, Yu S, Tanyi J, Lu Y, Woodgett J, Mills G (2002). Convergence of multiple signaling cascades at glycogen synthase kinase 3: Edg receptor-mediated phosphorylation and inactivation by lysophosphatidic acid through a protein kinase C-dependent intracellular pathway. Mol Cell Biol 22: 2099–2110.

Garlid KD, Costa AD, Quinlan CI, Pierre SV, Dos Santos P (2009). Cardioprotective signaling to mitochondria. J Mol Cell Cardiol 46: 858–866.

Gross E, Hsu A, Gross G (2004). Opioid-induced cardioprotection occurs via glycogen synthase kinase beta inhibition during reperfusion in intact rat hearts. Circ Res 94: 960–966.

Homans DC, Pavek T, Laxson DD, Bache RJ (1994). Recovery of transmural and subepicardial wall thickening after subendocardial infarction. J Am Coll Cardiol 24: 1109–1116.

Huang W, Chen Y, Shohami E, Weinstock M (1999). Neuroprotective effect of rasagiline, a selective monoamine oxidase-B inhibitor, against closed head injury in the mouse. Eur J Pharmacol 366: 127–135.

Inagaki K, Churchill E, Mochly-Rosen D (2006). Epsilon protein kinase C as a potential therapeutic target for the ischemic heart. Cardiovasc Res 70: 222–230.

Juhaszova M, Zorov D, Kim S, Pepe S, Fu Q, Fishbein K *et al.* (2004). Glycogen synthase kinase-3beta mediates convergence of protection signaling to inhibit the mitochondrial permeability transition pore. J Clin Invest 113: 1535–1549.

Juhaszova M, Zorov D, Yaniv Y, Nuss H, Wang S, Sollott S (2009). Role of glycogen synthase kinase-3beta in cardioprotection. Circ Res 104: 1240–1252.

Kleiner Y, Bar-Am O, Amit T, Berdichevski A, Liani E, Maor G *et al.* (2008). TVP1022 and propargylamine protect neonatal rat ventricular myocytes against doxorubicin-induced and serum starvation-induced cardiotoxicity. J Cardiovasc Pharmacol 52: 268–277.

Liu W, Ashford MW, Chen J, Watkins MP, Williams TA, Wickline SA *et al.* (2006). MR tagging demonstrates quantitative differences in regional ventricular wall motion in mice, rats, and men. Am J Physiol Heart Circ Physiol 291: H2515–H2521.

Lloyd-Jones D, Adams R, Carnethon M, De Simone G, Ferguson TB, Flegal K *et al.* (2009). American Heart Association Statistics Committee and Stroke Statistics Subcommittee. Heart disease and stroke statistics – 2009 update: a report from the American Heart Association Statistics Committee and Stroke Statistics Subcommittee. Circulation 27: 480–486.

Mandel S, Weinreb O, Amit T, Youdim M (2005). Mechanism of neuroprotective action of the anti-Parkinson drug rasagiline and its derivatives. Brain Res Brain Res Rev 48: 379–387.

Molavi B, Mehta J (2004). Oxidative stress in cardiovascular disease: molecular basis of its deleterious effects, its detection, and therapeutic considerations. Curr Opin Cardiol 19: 488–493.

Murphy K, Ranganathan V, Farnsworth M, Kavallaris M, Lock R (2000). Bcl-2 inhibits Bax translocation from cytosol to mitochondria during drug-induced apoptosis of human tumor cells. Cell Death Differ 7: 102–111.

Naoi M, Maruyama W (2009). Functional mechanism of neuroprotection by inhibitors of type B monoamine oxidase in Parkinson's disease. Expert Rev Neurother 9: 1233–1250.

Narita M, Shimizu S, Ito T, Chittenden T, Lutz R, Matsuda H *et al.* (1998). Bax interacts with the permeability transition pore to induce permeability transition and cytochrome c release in isolated mitochondria. Proc Natl Acad Sci USA 95: 14681–14686.

Ojha N, Roy S, Radtke J, Simonetti O, Gnyawali S, Zweier J *et al.* (2008). Characterization of the structural and functional changes in the myocardium following focal ischemia-reperfusion injury. Am J Physiol Heart Circ Physiol 294: H2435–H2443.

Onai Y, Suzuki J., Kakuta T, Maejima Y, Haraguchi G, Fukasawa H *et al.* (2004). Inhibition of IkappaB phosphorylation in cardiomyocytes attenuates myocardial ischemia/reperfusion injury. Cardiovasc Res 63: 51–59.

Pitts K, Stiko A, Buetow B, Lott F, Guo P, Virca D *et al.* (2007). Washout of heme-containing proteins dramatically improves tetrazolium-based infarct staining. J Pharmacol Toxicol Methods 55: 201–208.

Popovic Z, Benejam C, Bian J, Mal N, Drinko J, Lee K *et al.* (2007). Speckle-tracking echocardiography correctly identifies segmental left ventricular dysfunction induced by scarring in a rat model of myocardial infarction. Am J Physiol Heart Circ Physiol 292: H2809–H2816.

Porter A, Janicke R (1999). Emerging roles of caspase-3 in apoptosis. Cell Death Differ 6: 99–104.

Rappaport D, Adam D, Lysyansky P, Riesner S (2006). Assessment of myocardial regional strain and strain rate by tissue tracking in B-mode echocardiograms. Ultrasound Med Biol 32: 1181–1192.

Reinhardt C, Weinstein H, Wironen J, Leppo J (1993). Effect of triphenyl tetrazolium chloride staining on the distribution of radiolabeled pharmaceuticals. J Nucl Med 34: 1722–1727.

Sheng R, Gu Z, Xie M, Zhou W, Guo C (2010). Epigallocatechin gallate protects H9c2 cardiomyoblasts against hydrogen dioxides-induced apoptosis and telomere attrition. Eur J Pharmacol 641: 199–206.

Stein AB, Tiwari S, Thomas P, Hunt G, Levent C, Stoddard MF *et al.* (2007). Effects of anesthesia on echocardiographic assessment of left ventricular structure and function in rats. Basic Res Cardiol 102: 28–41.

Tiyyagura S, Pinney S (2006). Left ventricular remodeling after myocardial infarction: past, present, and future. Mt Sinai J Med 73: 840–851.

Umansky SR, Cuenco GM, Khutzian SS, Barr PJ, Tomei LD (1995). Post-ischemic apoptotic death of rat neonatal cardiomyocytes. Cell Death Differ 2: 235–241.

Wang G, Liem D, Vondriska T, Honda H, Korge P, Pantaleon D *et al*. (2005). Nitric oxide donors protect murine myocardium against infarction via modulation of mitochondrial permeability transition. Am J Physiol Heart Circ Physiol 288: H1290–H1295.

Weinreb O, Bar-Am O, Amit T, Chillag-Talmor O, Youdim M (2004). Neuroprotection via pro-survival protein kinase C isoforms associated with Bcl-2 family members. FASEB J 18: 1471–1473.

Weinreb O, Bar-Am O, Amit T, Drigues N, Sagi Y, Youdim M (2008). The neuroprotective effect of ladostigil against hydrogen peroxide-mediated cytotoxicity. Chem Biol Interact 175: 318–326.

Winstead MV, Lucas KK, Dennis EA (2005). Group IV cytosolic phospholipase A2 mediates arachidonic acid release in H9c2 rat cardiomyocyte cells in response to hydrogen peroxide. Prostaglandins Other Lipid Mediat 78: 55–66.

Youdim M, Gross A, Finberg J (2001). Rasagiline [N-propargyl-1R(+)-aminoindan], a selective and potent inhibitor of mitochondrial monoamine oxidase B. Br J Pharmacol 132: 500–506.

Youdim M, Bar Am O, Yogev-Falach M, Weinreb O, Maruyama W, Naoi M *et al*. (2005). Rasagiline: neurodegeneration, neuroprotection, and mitochondrial permeability transition. J Neurosci Res 79: 172–179.

Youn H, Kim H, Jeon M, Lee J, Seo Y, Lee Y *et al*. (2005). Induction of caspase-independent apoptosis in H9c2 cardiomyocytes by adriamycin treatment. Mol Cell Biochem 270: 13–19.

Zorov D, Juhaszova M, Yaniv Y, Nuss H, Wang S, Sollott S (2009). Regulation and pharmacology of the mitochondrial permeability transition pore. Cardiovasc Res 83: 213–225.